THE JOURNAL OF PHYSICAL CHEMISTRY Letters

pubs.acs.org/JPCL

Letter

The Prevalence of Anions at Plasmonic Nanojunctions: A Closer Look at *p*-Nitrothiophenol

Chih-Feng Wang, Brian T. O'Callahan, Dmitry Kurouski, Andrey Krayev, and Patrick Z. El-Khoury*

Cite This: *J. Phys. Chem. Lett.* 2020, 11, 3809−3814

Read Online

ACCESS | Metrics & More | Article Recommendations | Supporting Information

ABSTRACT: We revisit the reductive coupling of *p*-nitrothiophenol (NTP) to form dimercaptoazobenzene (DMAB), herein monitored through gap-mode tip-enhanced Raman spectroscopy (TERS) and nanoimaging. We employ a plasmonic Au probe (100 nm diameter at its apex) illuminated with a 633 nm laser source (50 $\mu W/\mu m^2$ at the sample position) to image an NTP-coated faceted silver nanoparticle (~70 nm diameter). A detailed analysis of the recorded spectra reveals that anionic NTP species contribute to the recorded spectral images, in addition to the more thoroughly described DMAB product. Notably, the signatures of the anions are more pronounced than those of the DMAB product under our present experimental conditions. Our results thus demonstrate that anions and their spectral signatures must be considered in the analysis of plasmon-enhanced optical spectra and images.

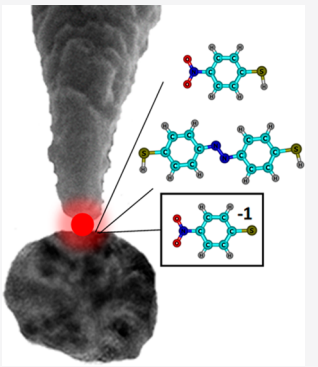

Monitoring chemical reactions at interfaces in real space (nanometer spatial resolution) and real time (femtosecond temporal resolution) continues to be one of the most sought-after quests in physical chemistry and chemical physics.[1] Plasmon-enhanced/induced molecular transformations in the immediate vicinity of plasmonic metals[2−8] are ideally suited for the aforementioned quest. This is because the same process, i.e., surface plasmon excitation through the resonant interaction between light and plasmonic metal nanostructures, can both induce chemistry and enhance molecular optical cross sections.[6] Surface and tip-enhanced Raman scattering (SERS[9−12] and TERS[13−15]) measurements that probe plasmon-enhanced/induced physical and chemical processes[16−18] are prime examples of how plasmons may be exploited to simultaneously drive and monitor chemical transformation with chemical selectivity, single-molecule detection sensitivity, and (ultra)high spatial resolution.[19−22]

The coupling reactions of 4-nitrothiophenol (NTP) and *p*-aminothiophenol (ATP) to form dimercaptoazobenzene (DMAB) on metallic substrates and nanostructures are prototypical plasmon-induced chemical transformations that have been thoroughly investigated by several groups.[23−26] Indeed, the DMAB product is routinely observed through SERS from ATP and NTP molecules chemisorbed onto various plasmonic substrates and nanoparticles.[23−27] Several fundamental investigations of the plasmon-induced dimerization process have also been performed to date; hot-electrons are generally implicated with the formation DMAB, which is marked by the appearance of characteristic Raman-active signatures of its azo moiety.[2,28−30] Using TERS, the NTP → DMAB transformation was also tracked in real-space by several groups.[16−18,31] In a pioneering study, Lantman et al. employed a combination of a 532/633 nm laser sources to induce/probe the dimerization process.[18] More recently, Kumar et al. reported TERS maps of DMAB formation at the solid−liquid interface using unique TERS probes that offer both strong Raman signal enhancement and stable operation in liquids.[17] Ren and co-workers carefully investigated the role of adsorption geometry/configuration and laser energies on the efficiency of the coupling reactions of NTP and ATP through a combination of TERS and density functional theory calculations.[31]

Despite the significant body of work that has been dedicated to understanding the prototypical plasmon-induced NTP → DMAB reaction, only a single report explored the formation of anionic NTP species at plasmonic nanojunctions.[32] This is surprising, as it is somewhat well-appreciated that the first step toward DMAB formation comprises the plasmon-induced reduction of NTP.[32,33] In a recent work, Kurouski and co-workers employed TERS to capture anionic NTP species on Au and to explore the mechanisms behind their formation.[32] The spatial sparsity and sporadic formation of the anions under the previous experimental conditions (Au−Au nanojunctions) nonetheless precluded capturing the full spectral features of the anions, their rigorous assignments, and quantitative analysis of

Received: March 30, 2020
Accepted: April 27, 2020
Published: April 27, 2020

https://dx.doi.org/10.1021/acs.jpclett.0c01006
J. Phys. Chem. Lett. 2020, 11, 3809−3814

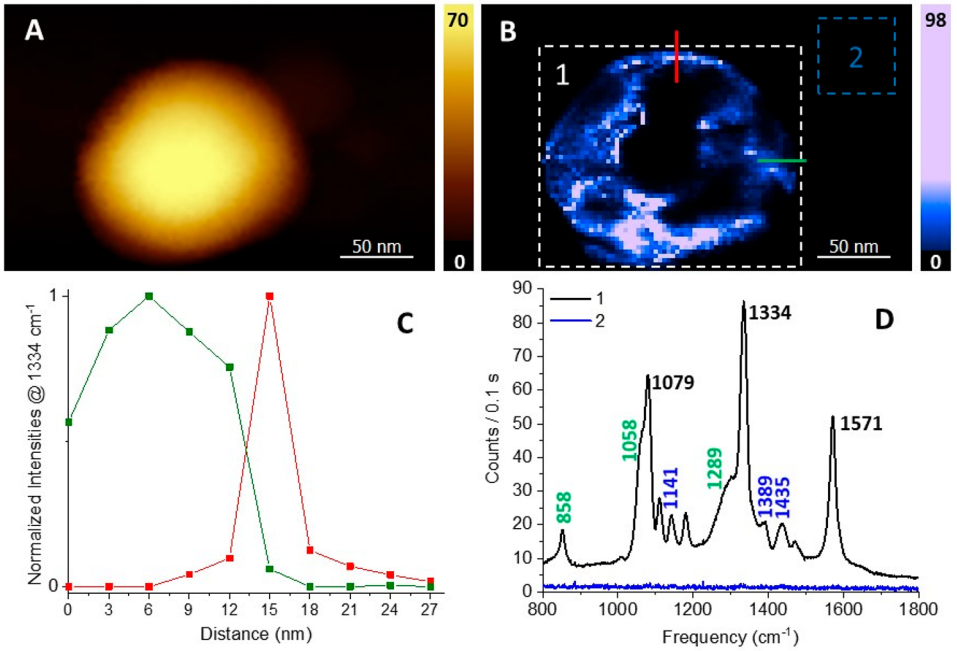

Figure 1. Simultaneously recorded AFM (A) and TERS (B) maps of an NTP-functionalized faceted silver nanoparticle. The TERS map is plotted at ∼1334 cm^{-1}, which can be assigned to the symmetric NO_2 stretching vibration of NTP. TERS cross-sectional cuts shown in panel B (highlighted using red vertical and green horizontal lines) are plotted in panel C to illustrate the attainable spatial resolution in our measurements. Spectra contained within the dashed rectangular areas (around the particle, 1, and off-particle, 2) in panel B were averaged, and the results are shown in panel D. Color-coded peak positions are also shown in panel D; their origin is deliberated in the ensuing sections of this work. Conditions used for TERS mapping: 50 $\mu W/\mu m^2$ at the sample position, 0.1 s time-integration at each pixel, 3 nm lateral steps.

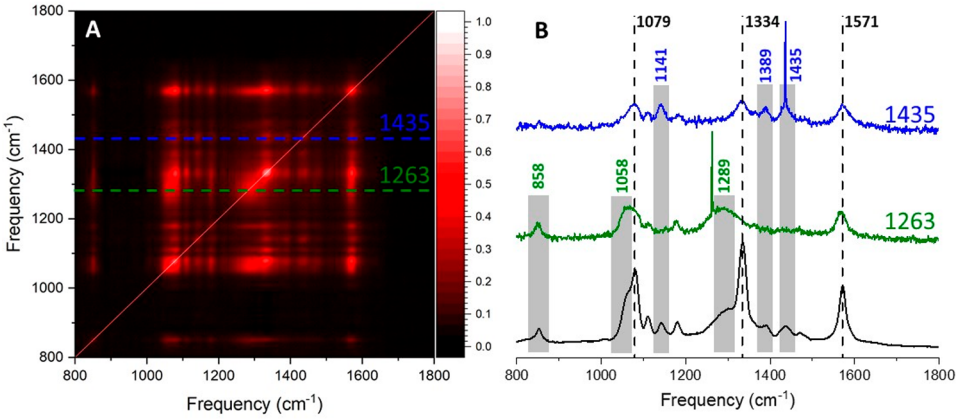

Figure 2. Cross-correlation map ($\rho_{j,k} = \sigma_{jk}^2/\sigma_{jj}\cdot\sigma_{kk}$) of the spectra contained in region 1 in Figure 1B. Cross-correlation slices ($\nu_j \neq \nu_k$) are taken at two frequencies (highlighted using green and blue dashed lines and numbers) and plotted along with the spatially averaged response in panel B. The highlighted regions (gray rectangles) highlight the contributions of two distinct species to the spatially averaged spectrum. Color-coded spectra and resonance maxima (consistent with their analogues in Figure 1D) are used throughout. Note that the dashed vertical lines highlight the 3 major resonances of NTP for reference. Also note that the spikes in the correlation slices (blue and green traces in Figure 2B) indicate positions at which the slices were taken; these are points at which diagonal correlations = 1.

their contributions to the recorded optical spectra and images.[32] The latter in part motivates our current work, which also builds on recent observations of anionic forms of a structurally related molecular system, 4-thiobenzonitirle (TBN), throughout the course of TERS mapping of TBN-functionalized plasmonic nanostructures[34] and nanoparticles.[35] For the purpose of this work, we utilize an NTP-coated faceted plasmonic silver nanoparticle to quantify the contributions of anionic NTP species to TERS spectra and images that we record using a Au TERS probe irradiated with a 633 nm laser source.

Figure 1 summarizes our general observations. Simultaneously recorded atomic force microscopy (AFM)-TERS maps of an NTP-coated silver nanoparticle are shown in panels A and B, respectively. The AFM map exposes the nonspherical morphology of the nanoparticle, but convolution with the tip radius (100 nm apex radius) limits further insights into its three-dimensional morphology based on this topographic image alone. The TERS map on the other hand is reminiscent of previously recorded TERS images of TBN-coated faceted silver nanoparticles.[36] Namely, the observation of similar spatial patterns that trace facet boundaries was associated with the general three-dimensional topographic makeups of

https://dx.doi.org/10.1021/acs.jpclett.0c01006
J. Phys. Chem. Lett. 2020, 11, 3809−3814

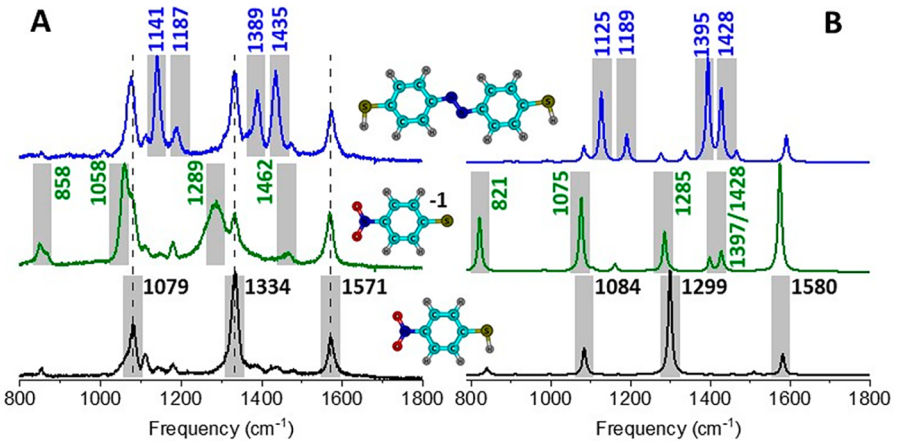

Figure 3. Experimental (A) and computed (B) Raman spectra of the parent, anion, and product. The experimental spectra are spatially averaged, as elaborated in the Supporting Information. The theoretical spectra were computed at the pbe/6-311++G** level of theory. The inset shows the optimized molecular structures of the models used to obtain the theoretical spectra.

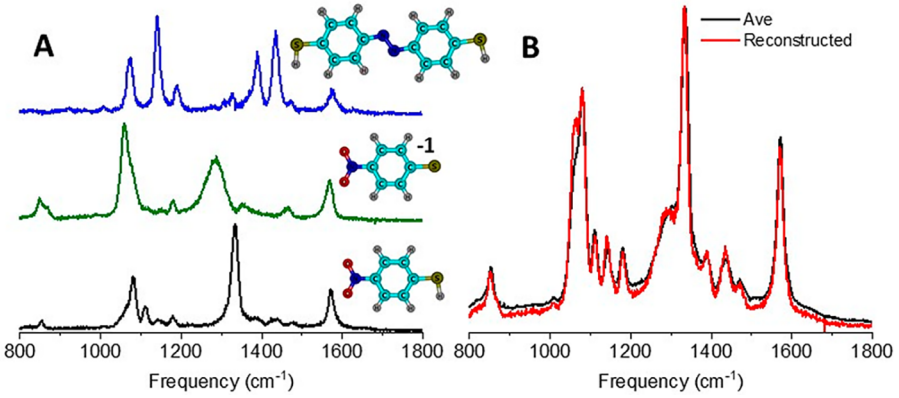

Figure 4. Pure parent, anion, and product spectra are shown in A. The latter two spectra were obtained by subtracting the contribution of the parent from the recorded product spectra (see Figure 3). In panel B, the average spectrum (see Figure 1) is plotted along with a reconstructed spectrum, obtained by scaling the contributions of NTP, the anion, and DMAB to the total response. More details on the latter are given in the main text.

faceted/nonuniform metallic nanoparticles. The case is perhaps best made by comparing TERS maps of faceted nanoparticles to Raman nanoimages of plasmonic nanocubes[36] and smooth spherical particles.[35] TERS cross-sectional cuts that illustrate our attainable spatial resolution are shown in Figure 1C. Consistent with prior TERS maps of similar chemically functionalized plasmonic constructs,[36] we can infer a (pixel-limited) sub-3 nm spatial resolution in our present measurements.

Spatially averaged spectra taken when the tip is atop versus in the immediate vicinity of the nanoparticle (see Figure 1B) are shown in Figure 1D. Besides the evident on- versus off-particle contrast, we note that no far-field (SERS) signals from the tip or nanoparticle are observable under our experimental conditions, even though the entire field of view is irradiated with the incident laser (objective NA = 0.7). The spectra themselves contain several spectral features that can be assigned to NTP (black numbers),[16] DMAB (blue numbers),[16] and anionic NTP (green numbers),[32] as further elaborated in the ensuing sections.

To rigorously establish the relationships between the different lines that contribute to the spatially averaged TERS response (see Figure 1D), we performed a 2D correlation analysis[37] of all spectra contained within region 1 in Figure 1B. The cross-correlation between the intensities of two resonances in the spectrum is given by

$$\chi_{j,k} = \frac{\sigma_{jk}}{\sqrt{\sigma_{jj}}\sqrt{\sigma_{kk}}}$$

in which σ_{jk} is the covariance and σ_{jj} and σ_{kk} are the statistical variances at frequencies j and k. Inspection of the 2D correlation map and correlation slices taken at select resonances in Figure 2 reveals that two distinct species (other than NTP) contribute to the recorded spectra. A correlation slice at 1435 cm^{-1} near the resonance maximum of the N=N stretching vibration of DMAB reveals all major resonances of the product,[16] which are all correlated as they arise from the same species. On the other hand, a correlation slice taken at 1272 cm^{-1}, near the maximum of the low-frequency (broad) shoulder of the predominant NTP Raman band (~1334 cm^{-1}) reveals at least three major peaks that are positively correlated. Prior assignments[32] of the anionic form of NTP predominantly relied on a single peak that appears toward the low-frequency shoulder of 1334 cm^{-1} band to establish anion formation. Below, we describe more general spectral characteristics of the anion and quantify its contribution to the total spatiotemporally averaged TERS response. At this juncture, the reader is referred to the

https://dx.doi.org/10.1021/acs.jpclett.0c01006
J. Phys. Chem. Lett. 2020, 11, 3809−3814

Supporting Information section of this work, wherein we take advantage of the above analysis to capture the NTP parent, DMAB product, and anionic NTP spectra. Briefly, the latter involved plotting the TERS images at the resonance maxima of the three species (identified in Figure 2B) followed by selecting the 15 brightest spectra that contribute to the three images.

Averaging the TERS response over the 15 brightest pixels that contribute to the parent, anion, and product maps yields the spectra shown in Figure 3A. Note that the spectra are normalized and stacked herein for illustrative purposes. Both individual spectra that contribute to the averaged response in all three cases as well as absolute counts are given in Supporting Information. Using simple molecular models of the isolated parent (NTP), anion (thiolate, charge/multiplicity = −1/1), and DMAB species, we are able to account for the majority of the dominant Raman-active vibrational states for each species through density functional theory simulations (see Figure 3B) that are described elsewhere.[16,32] A comparison between the experimental spectra themselves and the experimental versus theoretical spectra readily reveals that anionic NTP and DMAB spectra also contain characteristic signatures of the parent NTP molecules. In Figure 4, we show the "pure" anionic NTP and DMAB spectra, which we obtain by scaling and subtracting the contributions of the parent to these two spectra. The obtained DMAB spectrum is fully consistent with previously reported spectra of the same species.[16] The full spectral features of the anionic species in the 800−1800 cm^{-1} are also visible in Figure 4A, herein for the first time.

Having established the spectral features of all three species, our final question has to do with the relative contributions of the three species to our recorded TERS map. The latter is motivated by (i) the fact that several groups have not observed (or have not assigned) the anion throughout the course of SERS and TERS measurements of NTP and (ii) a recent work that shows that the contribution of the anion at plasmonic Au−Au nanojunction in the TERS scheme is not significant.[32] To this end, we weigh the pure NTP, anion, and DMAB spectra by their relative scattering activities under the identical conditions used to record our TERS map (see Supporting Information): 0.7:1:0.5 for the parent:anion:DMAB product. We then solve a linear equation to gauge the contributions of all three species to the spatially averaged spectrum. We find that the spatially averaged spectrum can be reconstructed with ∼64.5%, ∼21.3%, and ∼14.2% contributions from the parent, anion, and product spectra, respectively (see Figure 4B). To our surprise, the anion contributes more significantly to the response than the product under our experimental conditions. The fidelity of the reconstructed spectrum (Figure 4B) also confirms that (i) only three species contribute to the spatially averaged spectrum, which is consistent with our 2D correlation analysis, and (ii) the optical response from a few pixels (or TERS hotspots) dominates in the average that was taken over a much larger area (see Figure 1B).

The general observations described thus far are reproducible. In the Supporting Information section, we repeat the same measurements described throughout this work using different TERS probes and different plasmonic silver nanostructures (cubes). Several conclusions are therefore unavoidable based on our results and analyses. As a general statement, redox reactions and ionic species have to be more carefully considered in the analysis of SERS and TERS measurements, particularly those aimed at gauging plasmon-induced chemical transformations through Raman scattering. Besides multipolar Raman scattering in the TERS geometry, which we have recently described in some detail,[38] and consistent with several recent reports from our group,[32,34,35] anions seem to be commonly encountered throughout the course of TERS nanoimaging and nanospectroscopy. Herein, the anionic NTP species is, on average, more frequently sampled than the DMAB product (or features a higher scattering cross-section). Spatially averaged parent, anion, and product spectra recorded under identical experimental conditions further reveal that the anionic form features the strongest Raman scattering cross section among the three species under our present experimental conditions. On a technical note, and in addition to the fundamental interest in tracking chemical reactions in real space, anion and product formation may be considered "parasitic" in cases where parent mapping is the ultimate goal. In this regard, it would be useful to develop approaches that may be used to control/suppress chemistry throughout the course of TERS mapping. This is not to say that the rich physics and chemistry that is broadcasted through TERS is not exciting in itself, but rather to stress the pressing need for noninvasive (in the chemical sense) analytical TERS nanoscopy and nano-imaging.

METHODS

A thin layer of 0.001% ethanolic PAMAM (Sigma-Aldrich) solution was spin-cast onto a silicon chip at 2000 rpm and allowed to sit for 1 min. Stock solutions (20 μL) of 100/75 nm silver nanoparticles/nanocubes (both from Sigma-Aldrich) were subsequently deposited onto the PAMAM-coated substrate. After the drop was air-dried, the substrate was washed with excess amounts of ethanol. A 20 μL volume of a 1 mM ethanolic solution of NTP was then deposited onto nanoparticles dispersed in a PAMAM matrix. Excess NTP was washed off with ample amounts of ethanol, and the final sample was dried using a stream of nitrogen.

Our TERS setup is described elsewhere in great detail.[34−36] For the purpose of this work, silicon probes (Nanosensors, ATEC) coated with 100 nm of gold were used for AFM (tapping mode feedback) and TERS (intermittent contact feedback) topographic/chemical imaging. For the latter, TERS signals were collected when the tip was in direct contact with the surface. A semicontact mode is otherwise used to move the sample relative to the tip (pixel to pixel). For TERS measurements, a 633 nm laser (∼50 μW) is focused onto the tip apex at a ∼65° angle with respect to the surface normal using a 100× air objective (Mitutoyo, 0.7 NA). The polarization of the laser was set along the tip axis using a half-waveplate. The backscattered light was collected using the same objective, filtered through a series of long pass filters, and recorded using a CCD camera (Andor, Newton EMCCD) coupled to a spectrometer (Andor, Shamrock 500) equipped with a 300 l/mm grating blazed at 550 nm.

ASSOCIATED CONTENT

Supporting Information

The Supporting Information is available free of charge at https://pubs.acs.org/doi/10.1021/acs.jpclett.0c01006.

Protocol used to identify the brightest parent, anion, and product signatures that contribute to TERS maps; corresponding plots of individual pixel spectra and

https://dx.doi.org/10.1021/acs.jpclett.0c01006
J. Phys. Chem. Lett. 2020, 11, 3809−3814

their averages; coarse TERS maps of NTP-coated Ag nanocubes that were recorded using two different TERS probes (PDF)

AUTHOR INFORMATION

Corresponding Author

Patrick Z. El-Khoury − *Physical Sciences Division, Pacific Northwest National Laboratory, Richland, Washington 99352, United States;* orcid.org/0000-0002-6032-9006; Email: patrick.elkhoury@pnnl.gov

Authors

Chih-Feng Wang − *Physical Sciences Division, Pacific Northwest National Laboratory, Richland, Washington 99352, United States;* orcid.org/0000-0002-3085-6614

Brian T. O'Callahan − *Earth and Biological Sciences Division, Pacific Northwest National Laboratory, Richland, Washington 99352, United States;* orcid.org/0000-0001-9835-3207

Dmitry Kurouski − *Department of Biochemistry and Biophysics, Texas A&M University, College Station, Texas 77843, United States;* orcid.org/0000-0002-6040-4213

Andrey Krayev − *Horiba Instruments Inc., Novato, California 94949, United States*

Complete contact information is available at: https://pubs.acs.org/10.1021/acs.jpclett.0c01006

Notes

The authors declare no competing financial interest.

ACKNOWLEDGMENTS

C.F.W. and B.T.O. were supported by the US Department of Energy (DOE), Office of Science, Office of Biological and Environmental Research through the bioimaging technology development program. P.Z.E. was supported by the US DOE, Office of Science, Office of Basic Energy Sciences, Division of Chemical Sciences, Geosciences & Biosciences. A portion of the research was performed using EMSL, a DOE Office of Science User Facility sponsored by the Office of Biological and Environmental Research and located at the Pacific Northwest National Laboratory (PNNL). PNNL is operated by Battelle Memorial Institute for the United States Department of Energy under DOE Contract Number DE-AC05-76RL1830.

REFERENCES

(1) Petek, H. Single-Molecule Femtochemistry: Molecular Imaging at the Space-Time Limit. *ACS Nano* **2014**, *8*, 5−13.

(2) Kazuma, E.; Kim, Y. Mechanistic Studies of Plasmon Chemistry on Metal Catalysts. *Angew. Chem., Int. Ed.* **2019**, *58*, 4800−4808.

(3) Su, M. N.; Sun, Q.; Ueno, K.; Chang, W. S.; Misawa, H.; Link, S. Optical Characterization of Gold Nanoblock Dimers: From Capacitive Coupling to Charge Transfer Plasmons and Rod Modes. *J. Phys. Chem. C* **2018**, *122*, 18005−18011.

(4) Link, S.; Masiello, D. J. Introduction: Plasmonics in Chemistry. *Chem. Rev.* **2018**, *118*, 2863−2864.

(5) Zhou, L.; et al. Quantifying Hot Carrier and Thermal Contributions in Plasmonic Photocatalysis. *Science* **2018**, *362*, 69−72.

(6) Zhan, C.; Chen, X. J.; Yi, J.; Li, J. F.; Wu, D. Y.; Tian, Z. Q. From Plasmon-Enhanced Molecular Spectroscopy to Plasmon-Mediated Chemical Reactions. *Nat. Rev. Chem.* **2018**, *2*, 216−230.

(7) Christopher, P.; Moskovits, M. Hot Charge Carrier Transmission from Plasmonic Nanostructures. *Annu. Rev. Phys. Chem.* **2017**, *68*, 379−398.

(8) Brongersma, M. L.; Halas, N. J.; Nordlander, P. Plasmon-Induced Hot Carrier Science and Technology. *Nat. Nanotechnol.* **2015**, *10*, 25−34.

(9) Fleischmann, M.; Hendra, P. J.; Mcquillan, A. J. Raman-Spectra of Pyridine Adsorbed at a Silver Electrode. *Chem. Phys. Lett.* **1974**, *26*, 163−166.

(10) Jeanmaire, D. L.; Van Duyne, R. P. Surface Raman Spectroelectrochemistry 0.1. Heterocyclic, Aromatic, and Aliphatic-Amines Adsorbed on Anodized Silver Electrode. *J. Electroanal. Chem. Interfacial Electrochem.* **1977**, *84*, 1−20.

(11) Moskovits, M. Surface-Roughness and Enhanced Intensity of Raman-Scattering by Molecules Adsorbed on Metals. *J. Chem. Phys.* **1978**, *69*, 4159.

(12) Otto, A. Raman-Spectra of Cn^- Adsorbed at a Silver Surface. *Surf. Sci.* **1978**, *75*, L392−L396.

(13) Anderson, M. S. Locally Enhanced Raman Spectroscopy with an Atomic Force Microscope. *Appl. Phys. Lett.* **2000**, *76*, 3130−3132.

(14) Stockle, R. M.; Suh, Y. D.; Deckert, V.; Zenobi, R. Nanoscale Chemical Analysis by Tip-Enhanced Raman Spectroscopy. *Chem. Phys. Lett.* **2000**, *318*, 131−136.

(15) Pettinger, B.; Schambach, P.; Villagómez, C. J.; Scott, N. Tip-Enhanced Raman Spectroscopy: Near-Fields Acting on a Few Molecules. *Annu. Rev. Phys. Chem.* **2012**, *63*, 379−399.

(16) Bhattarai, A.; El-Khoury, P. Z. Nanoscale Chemical Reaction Imaging at the Solid−Liquid Interface Via Ters. *J. Phys. Chem. Lett.* **2019**, *10*, 2817−2822.

(17) Kumar, N.; Su, W. T.; Vesely, M.; Weckhuysen, B. M.; Pollard, A. J.; Wain, A. J. Nanoscale Chemical Imaging of Solid-Liquid Interfaces Using Tip-Enhanced Raman Spectroscopy. *Nanoscale* **2018**, *10*, 1815−1824.

(18) van Schrojenstein Lantman, E. M.; Deckert-Gaudig, T.; Mank, A. J. G.; Deckert, V.; Weckhuysen, B. M. Catalytic Processes Monitored at the Nanoscale with Tip-Enhanced Raman Spectroscopy. *Nat. Nanotechnol.* **2012**, *7*, 583−586.

(19) He, Z.; et al. Tip-Enhanced Raman Imaging of Single-Stranded DNA with Single Base Resolution. *J. Am. Chem. Soc.* **2019**, *141*, 753−757.

(20) Zhang, R.; et al. Chemical Mapping of a Single Molecule by Plasmon-Enhanced Raman Scattering. *Nature* **2013**, *498*, 82−86.

(21) Lee, J.; Crampton, K. T.; Tallarida, N.; Apkarian, V. A. Visualizing Vibrational Normal Modes of a Single Molecule with Atomically Confined Light. *Nature* **2019**, *568*, 78−82.

(22) Pozzi, E. K.; et al. Ultrahigh-Vacuum Tip-Enhanced Raman Spectroscopy. *Chem. Rev.* **2017**, *117*, 4961−4982.

(23) Huang, Y. F.; Zhu, H. P.; Liu, G. K.; Wu, D. Y.; Ren, B.; Tian, Z. Q. When the Signal Is Not from the Original Molecule to Be Detected: Chemical Transformation of Para-Aminothiophenol on Ag During the Sers Measurement. *J. Am. Chem. Soc.* **2010**, *132*, 9244−9246.

(24) Kim, K.; Shin, D.; Lee, H. B.; Shin, K. S. Surface-Enhanced Raman Scattering of 4-Aminobenzenethiol on Gold: The Concept of Threshold Energy in Charge Transfer Enhancement. *Chem. Commun.* **2011**, *47*, 2020−2022.

(25) Zhao, L. B.; Huang, Y. F.; Liu, X. M.; Anema, J. R.; Wu, D. Y.; Ren, B.; Tian, Z. Q. A Dft Study on Photoinduced Surface Catalytic Coupling Reactions on Nanostructured Silver: Selective Formation of Azobenzene Derivatives from Para-Substituted Nitrobenzene and Aniline. *Phys. Chem. Chem. Phys.* **2012**, *14*, 12919−12929.

(26) Choi, H. K.; Park, W. H.; Park, C. G.; Shin, H. H.; Lee, K. S.; Kim, Z. H. Metal-Catalyzed Chemical Reaction of Single Molecules Directly Probed by Vibrational Spectroscopy. *J. Am. Chem. Soc.* **2016**, *138*, 4673−4684.

(27) Nelson, D. A.; Schultz, Z. D. Influence of Optically Rectified Electric Fields on the Plasmonic Photocatalysis of 4-Nitrothiophenol and 4-Aminothiophenol to 4,4-Dimercaptoazobenzene. *J. Phys. Chem. C* **2018**, *122*, 8581−8588.

(28) Zhang, Z. L.; Deckert-Gaudig, T.; Singh, P.; Deckert, V. Single Molecule Level Plasmonic Catalysis - a Dilution Study of P-

Nitrothiophenol on Gold Dimers. *Chem. Commun.* **2015**, *51*, 3069−3072.
(29) Brandt, N. C.; Keller, E. L.; Frontiera, R. R. Ultrafast Surface-Enhanced Raman Probing of the Role of Hot Electrons in Plasmon-Driven Chemistry. *J. Phys. Chem. Lett.* **2016**, *7*, 3179−85.
(30) Zhang, Z. L.; Kinzel, D.; Deckert, V. Photo-Induced or Plasmon-Induced Reaction: Investigation of the Light-Induced Azo-Coupling of Amino Groups. *J. Phys. Chem. C* **2016**, *120*, 20978−20983.
(31) Sun, J. J.; Su, H. S.; Yue, H. L.; Huang, S. C.; Huang, T. X.; Hu, S.; Sartin, M. M.; Cheng, J.; Ren, B. Role of Adsorption Orientation in Surface Plasmon-Driven Coupling Reactions Studied by Tip-Enhanced Raman Spectroscopy. *J. Phys. Chem. Lett.* **2019**, *10*, 2306−2312.
(32) Wang, R.; Li, J. B.; Rigor, J.; Large, N.; El-Khoury, P. Z.; Rogachev, A. Y.; Kurouski, D. Direct Experimental Evidence of Hot Carrier-Driven Chemical Processes in Tip-Enhanced Raman Spectroscopy (Ters). *J. Phys. Chem. C* **2020**, *124*, 2238−2244.
(33) Zhao, L. B.; Chen, J. L.; Zhang, M.; Wu, D. Y.; Tian, Z. Q. Theoretical Study on Electroreduction of P-Nitrothiophenol on Silver and Gold Electrode Surfaces. *J. Phys. Chem. C* **2015**, *119*, 4949−4958.
(34) Bhattarai, A.; Crampton, K. T.; Joly, A. G.; Wang, C. F.; Schultz, Z. D.; El-Khoury, P. Z. A Closer Look at Corrugated Au Tips. *J. Phys. Chem. Lett.* **2020**, *11*, 1915−1920.
(35) Bhattarai, A.; Cheng, Z.; Joly, A. G.; Novikova, I. V.; Evans, J. E.; Schultz, Z. D.; Jones, M. R.; El-Khoury, P. Z. Tip-Enhanced Raman Nanospectroscopy of Smooth Spherical Gold Nanoparticles. *J. Phys. Chem. Lett.* **2020**, *11*, 1795−1801.
(36) Bhattarai, A.; Novikova, I. V.; El-Khoury, P. Z. Tip-Enhanced Raman Nanographs of Plasmonic Silver Nanoparticles. *J. Phys. Chem. C* **2019**, *123*, 27765−27769.
(37) Noda, I.; Ozaki, Y. *Two-Dimensional Correlation Spectroscopy: Applications in Vibrational and Optical Spectroscopy*; John Wiley and Sons, Ltd.: Chichester, U.K., 2004.
(38) Wang, C. F.; Cheng, Z.; O'Callahan, B. T.; Crampton, K. T.; Jones, M. R.; El-Khoury, P. Z. Tip-Enhanced Multipolar Raman Scattering. *J. Phys. Chem. Lett.* **2020**, *11*, 2464−2469.

https://dx.doi.org/10.1021/acs.jpclett.0c01006
J. Phys. Chem. Lett. 2020, 11, 3809−3814